Effect of Ni impurities on the optical properties of $YBa_2Cu_3O_{6+y}$

C. C. Homes*
Department of Physics, Brookhaven National Laboratory, Upton, New York 11973-5000

D. A. Bonn, Ruixing Liang, and W. N. Hardy
Department of Physics and Astronomy, University of British Columbia, Vancouver, British Columbia, Canada V6T 1Z1

D. N. Basov
Department of Physics, University of California at San Diego, La Jolla, California 92093-0319

T. Timusk
Department of Physics and Astronomy, McMaster University, Hamilton, Ontario, Canada L8S 4M1

B. P. Clayman
Department of Physics, Simon Fraser University, Burnaby, British Columbia, Canada V5A 1S6
(Received 23 February 1999)

The optical properties of twinned single crystals of $YBa_2(Cu_{1-x}Ni_x)_3O_{6+y}$ have been determined for a nominally pure system and for Ni concentrations of $x=0.0075$ and 0.014 with oxygen dopings of $y=0.60$ (underdoped) and 0.95 (optimal) over a wide frequency range above and below T_c. The optical conductivity of the twinned materials shows a rapid increase in the residual conductivity at low frequency with increasing Ni concentration, and an unusual feature appears below T_c at ≈ 300 cm^{-1} (37 meV), which is absent in the pure system and is not sensitive upon oxygen content. In a detwinned crystal of the optimally doped system this Ni-induced feature is observed only along the *b* axis, suggesting that Ni is doping into the chains. Since the feature is observed in the normal state, it is not associated with the superconducting transition. The free-carrier response in the CuO_2 planes is quite different in the optimally doped and underdoped materials. The presence of Ni in these materials has little effect upon the in-plane dynamics, but the low-frequency conductivity along just the chains is destroyed. This suggests that Ni acts either as a localization site, or an impurity scatterer and strong pair breaker, destroying the superconductivity along the chains and strongly reducing the anisotropy of the system at low frequency. The feature at ≈ 300 cm^{-1} along the chain direction is most likely due to the Ni impurities acting as strong scattering barriers, resulting in thermally activated hopping. However, the proximity of this feature to the estimated value of the *c*-axis pseudogap in the underdoped materials also suggests that strong scattering out of the chains may be coupling to the *c*-axis dynamics. [S0163-1829(99)00537-8]

I. INTRODUCTION

Since the discovery of superconductivity at high temperatures, $YBa_2Cu_3O_{7-\delta}$ has been one of the most thoroughly investigated systems.[1–4] While the presence of CuO chains creates an added degree of complexity in this material, refinements in growth techniques[5] have allowed the intrinsic properties (which strongly suggest an unconventional *d*-wave symmetry of the order parameter[6,7]) to be distinguished from the extrinsic effects due to impurities.[8] This serves as a natural motivation to study the optical properties of nominally pure systems in comparison to systems into which impurities have been selectively introduced. For instance, it has been proposed that impurity doping in the CuO_2 planes of the high-T_c superconductors may also allow a distinction between *d* wave and the various *s*-wave models.[9–11] A comparison between the effects of Ni and Zn doping in $YBa_2Cu_3O_{7-\delta}$ shows that while both Ni and Zn are effective scatters in the normal state and preserve the linear temperature dependence of the resistivity,[12–15] Zn reduces T_c about three times more quickly than Ni.[16] There is some evidence that the rapid reduction of T_c due to Zn doping may be related to magnetic effects.[17,18]

It is primarily because of this anomalous effect upon T_c that optical studies of impurity effects in single crystals of $YBa_2Cu_3O_{7-\delta}$ and $YBa_2Cu_4O_8$ have been restricted so far to Zn doping.[19–21] While there is no unusual structure at low frequency that could be attributed to a gap, there is some evidence in the mid-infrared region (≈ 2000 cm^{-1}) for carrier localization along the chains due to impurity defects,[19] which has also been observed in early work on (undoped) detwinned, oxygen-reduced systems.[22] A larger body of work exists of studies of Ni and Zn-doped $YBa_2Cu_3O_{6.95}$ thin films.[12,13]

In this paper, we report on the effects of Ni doping on the optical properties of twinned, single crystals of $YBa_2(Cu_{1-x}Ni_x)_3O_{6+y}$ with optimal oxygen doping ($y=0.95$) over a wide frequency range, above and below T_c for a pure system ($x=0$), a material with a light Ni concentration ($x=0.0075$), and a heavy Ni concentration ($x=0.014$). In addition, the crystal with the lighter Ni concentration has been mechanically detwinned and studied at both the optimal oxygen doping, and in the underdoped ($y=0.60$) regime, for light polarized along the *a* and *b* axes

and is compared to nominally pure material with the same oxygen content. The selective introduction of impurities is preferable to other techniques such as radiation damage,[23] which introduce scattering sites throughout the crystal. However, Ni is thought to substitute preferentially into the Cu(2) plane sites in $YBa_2Cu_3O_{7-\delta}$ crystal structure,[24] [although there has been some evidence of Ni doping into the Cu(1) chain sites as well[25,26]] thus providing a well-controlled means of studying the effects of impurities in the CuO_2 planes, which are the common element to all of the cuprate superconductors. A preliminary report on the results of the lightly doped crystal with optimal oxygen doping has been previously published.[27]

The temperature and frequency dependence of the optical conductivity of the nominally pure twinned system is similar to previous studies.[3] However, the low-frequency residual conductivity increases rapidly with Ni doping above and below T_c. In addition a shoulder in the conductivity (not seen in the undoped systems) is observed at $\approx 300\ \mathrm{cm}^{-1}$ for $T \ll T_c$.

In the detwinned crystal with the light Ni concentration at optimal oxygen doping, the shoulder is observed only along the *b* axis, the direction of the CuO chains, and not in the *a* direction. In addition, this feature is observed in the normal state above T_c, as well as below T_c, indicating that it is not associated with the superconducting transition in this material. While there is a great deal more residual conductivity at low frequencies along the chain direction, Ni doping has little effect upon the CuO_2 planes. In the oxygen-underdoped material with the same Ni concentration, a similar behavior along the chain direction is observed. While Ni incorporation has relatively little effect on the CuO_2 planes, the normal-state dynamics is quite different in the optimally doped and oxygen underdoped materials. The possible origins of the shoulder at $\approx 300\ \mathrm{cm}^{-1}$ due to thermally-activated hopping in the chains (or possibly strong scattering out of the chains into the bilayers) will be discussed, as well as the more general aspects of the optical properties that evolve not only with Ni incorporation, but also with oxygen doping.

II. EXPERIMENT AND SAMPLE PREPARATION

High quality, twinned single crystals of $YBa_2(Cu_{1-x}Ni_x)_3O_{6.95}$ were grown using a flux technique[5] for $x=0.0$, 0.0075, and 0.014 (''pure,'' ''light,'' and ''heavy'' nickel concentrations). The crystals were post annealed in a furnace under high-purity oxygen flow at 860 °C for 48 h, then slowly cooled to 450 °C and reannealed for a week. The crystals had optically flat surfaces and were typically 1.0×1.5 mm in the *a-b* plane, but only $\approx 50\ \mu$m along the *c* axis. The pure crystal shows a narrow transition in susceptibility ($\leqslant 0.5$ K) at 93.2 K, while the light and heavy Ni concentrations show somewhat broader transitions ($\leqslant 0.9$,1.1 K) at 91 and 89 K, respectively. A pure crystal with optimal oxygen doping from the same group has been mechanically detwinned, allowing the optical properties along the *a* and *b* axes to be studied. In the course of these experiments, the crystal with the light Ni concentration and optimal oxygen doping was also mechanically detwinned (this crystal is referred to as ''RL1138'' in the plots). The crystals were first detwinned using uniaxial stress, and then reannealed in flowing oxygen at 450 °C for a week. This temperature is low enough so that there is negligible retwinning, unless there are strains present in the sample. Samples were checked for signs of retwinning by examining them under a microscope using polarized light.

The oxygen-underdoped materials have also been examined. Both a nominally pure sample and the detwinned sample with the light Ni concentration (RL1138) of $YBa_2Cu_3O_{6.95}$, were first annealed at 700 °C in order to reduce the oxygen content. After quenching to room temperature, the crystals were detwinned under uniaxial stress. The crystals were then sealed in a quartz tube along with some $YBa_2Cu_3O_{6+y}$ powder that had also been treated to produce an oxygen content of $y=0.6$ (Ref. 28). The crystals and the powder are then annealed together at 390 °C to ensure that the crystals have a homogeneous oxygen content of $y=0.6$, without going to high enough temperatures to cause retwinning. (Note that the samples were again checked for signs of retwinning under a polarizing microscope.) The twinned crystal with the highest Ni concentration was also oxygen reduced; however, this sample was not detwinned.

The crystals were mounted on optically black cones, and the reflectance was measured from ≈ 40–$9000\ \mathrm{cm}^{-1}$ on a Bruker IFS 113v using an *in situ* overcoating technique, which has previously been described in detail elsewhere.[29] This technique is especially useful when measuring small samples, as it allows the entire face of the sample to be utilized. The measurements of the pure, detwinned $YBa_2Cu_3O_{6.95}$ and oxygen-reduced $YBa_2Cu_3O_{6.60}$ samples were performed at McMaster using the same technique with a custom-built interferometer. While the uncertainty of the reflectance of the gold reference limits the accuracy of the absolute value of the reflectance to $\pm 0.5\%$, the noise in the reflectance is typically less than $\pm 0.1\%$. The optical conductivity has been determined from a Kramers-Kronig analysis of the reflectance, for which extrapolations to $\omega \rightarrow 0,\infty$ must be supplied. For $\omega \rightarrow 0$, the reflectance was extrapolated by assuming a Hagen-Rubens frequency dependence in the normal state, $(1-R) \propto \omega^{1/2}$; below T_c a $(1-R) \propto \omega^2$ extrapolation was used. When the reflectance approaches unity, the results in the region of the data are fairly insensitive to the type of low-frequency extrapolation employed.[30] The reflectance has been extended to high-frequency ($3.5 \times 10^5\ \mathrm{cm}^{-1}$) using the measurements of Romberg *et al.*[31] and Basov and co-workers[32,33] above which a free-electron behavior ($R \propto \omega^{-4}$) was assumed.

III. RESULTS

A. Twinned samples

The optical conductivity for twinned single crystals of nominally pure $YBa_2Cu_3O_{6.95}$ ($T_c=93.2$ K), $YBa_2(Cu_{1-x}Ni_x)_3O_{6.95}$ with a light Ni concentration of $x=0.0075$ ($T_c=91$ K), and a heavy Ni concentration of $x=0.014$ ($T_c=89$ K) are shown in Figs. 1(a), (b), and (c), respectively. The results in Fig. 1(a) are similar to other optical studies of twinned single crystals of $YBa_2Cu_3O_{7-\delta}$ (Refs. 3 and 4). At room temperature, the conductivity can be described in general terms as a Lorentzian centered at zero frequency (Drude component) with the contribution to

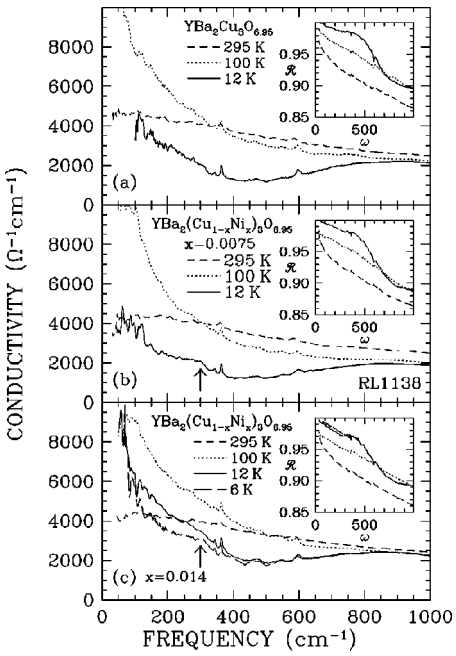

FIG. 1. (a) The optical conductivity $[\sigma_1(\omega)]$ for $YBa_2Cu_3O_{6.95}$ ($T_c=93.2$ K). Inset: the reflectance at 295, 100, and 12 K from $\approx$50–1000 cm^{-1}. (b) The optical conductivity for $YBa_2(Cu_{1-x}Ni_x)_3O_{6.95}$ for $x=0.0075$ ($T_c=91$ K). Note the shoulder in $\sigma_1(\omega)$ at $\approx$300 cm^{-1} below T_c. (c) The optical conductivity for $YBa_2(Cu_{1-x}Ni_x)_3O_{6.95}$ for $x=0.014$ ($T_c=89$ K). Note that the shoulder in $\sigma_1(\omega)$ is still visible at low temperature.

the optical conductivity in the midinfrared due to excitations of an unspecified nature. A general view of the free-carrier response includes a frequency dependence in the scattering rate and effective mass. This generalized Drude model or ''one component'' model has the complex dielectric function

$$\tilde{\epsilon}(\omega)=\epsilon_\infty-\frac{\omega_p^2}{\omega[m^*(\omega)/m][\omega+i\Gamma(\omega)]}, \tag{1}$$

where ω_p is the plasma frequency of the charge carriers, and $\Gamma(\omega)=1/\tau(\omega)$ and $m^*(\omega)/m$ describe the frequency dependent (unrenormalized) carrier scattering rate and effective mass enhancement over the bare (or optical) mass. The effective mass is also given by $m^*(\omega)=m[1+\lambda(\omega)]$, where $\lambda(\omega)$ is a frequency dependent renormalization. The complex conductivity is $\tilde{\sigma}(\omega)=-i\omega\tilde{\epsilon}(\omega)/(4\pi)$, which neglecting the contributions to the imaginary part due to ϵ_∞, is $\tilde{\sigma}(\omega)=\omega_p^2/\{4\pi[m^*(\omega)/m][\omega-i\Gamma(\omega)]\}$. The $1/\tau(\omega)$ and $\lambda(\omega)$ can be found experimentally[34] by

$$\frac{1}{\tau(\omega)}=\frac{\omega_p^2}{4\pi}\mathrm{Re}\left[\frac{1}{\tilde{\sigma}(\omega)}\right], \tag{2}$$

and

$$\frac{m^*(\omega)}{m}=1+\lambda(\omega)=\frac{\omega_p^2}{4\pi\omega}\mathrm{Im}\left[\frac{1}{\tilde{\sigma}(\omega)}\right]. \tag{3}$$

In the one-component model [Eq. (1)] there are no explicit contributions to the frequency dependent scattering rate and the effective-mass enhancement due to bound excitations. However, because these quantities are determined empirically, high frequencies will include the contributions to the dielectric function from the free carriers as well as the bound states. Consequently, the one-component model is typically applied only at low frequencies ($\omega\lesssim1000$ cm^{-1}).

In the pure sample shown in Fig. 1(a), as the temperature decreases from 300–100 K there is a dramatic narrowing of the free-carrier component and transfer of spectral weight to low frequencies. Well below T_c, at 12 K, $\sigma_1(\omega)$ is suppressed below $\approx$800 cm^{-1} reaching a minimum value of $\approx1100\ \Omega^{-1}$ cm^{-1} at $\approx$400 cm^{-1}; below this frequency a large amount of residual conductivity is observed and $\sigma_1(\omega)$ begins to increase with decreasing frequency. Superimposed on the smoothly varying conductivity are several sharp features which are associated with the normally active infrared vibrations of the lattice; these features will be examined in detail in a separate publication. The reflectance is shown in the inset in Fig. 1(a); it increases rapidly at low frequency with decreasing temperature, which is characteristic of a ''metallic'' response. In the superconducting state the reflectance is always less than unity to the lowest measured frequency ($\approx$50 cm^{-1}), indicating the presence of residual conductivity at low frequencies.

In the $YBa_2(Cu_{1-x}Ni_x)_3O_{6.95}$ material with the light Ni concentration of $x=0.0075$ ($T_c=91$ K) shown in Fig. 1(b), the behavior of $\sigma_1(\omega)$ is similar to that of the pure material above and below T_c. However, there is an unusual shoulder in $\sigma_1(\omega)$ at $\approx$300 cm^{-1} observed below T_c, seen as a ''bump'' or slight minimum at roughly the same position in the low-temperature reflectance.

In $YBa_2(Cu_{1-x}Ni_x)_3O_{6.95}$ material with the heavy Ni concentration of $x=0.014$ ($T_c=89$ K) shown in Fig. 1(c), the effects of nickel incorporation are quite prominent. While $\sigma_1(\omega)$ begins to decrease below $\approx$800 cm^{-1} below T_c, the minimum at $\approx$400 cm^{-1} is now far less pronounced (almost nonexistent), and the amount of residual conductivity at low frequency has increased dramatically to the point that at $\approx$12 K, the shoulder in $\sigma_1(\omega)$ is not clearly visible. However, at $\approx$6 K, the amount of low-frequency residual conductivity has decreased enough to allow the shoulder at $\approx$300 cm^{-1} to be distinguished. The feature at $\approx$300 cm^{-1} can be seen as a weak feature in the reflectance at roughly the same position below T_c. While the low-frequency reflectance increases below T_c, the fact that it is now noticeably less than in either the pure or lightly doped materials is due to the large amount of residual conductivity at low frequency below T_c.

We now turn to the calculation of the free-carrier spectral weight. We define spectral weight as $I(\omega)=(120/\pi)\int_0^\omega[\sigma_1(\omega')d\omega']$, where $\sigma_1(\omega)$ has the units of Ω^{-1} cm^{-1}; from the *f*-sum rule, in the absence of any bound excitations, $I(\omega\rightarrow\infty)=\omega_p^2$ (Ref. 35). Because of the non-Drude behavior of the free-carrier conductivity and the presence of interband absorptions it is necessary to choose an arbitrary cutoff, which we take as 1 eV. This frequency includes the mid-infrared band, but not the charge-transfer excitations that start at $\approx$1 eV (Ref. 36). In Fig. 2 the value for $I(\omega)$ is shown up to a value of 8000 cm^{-1} for $YBa_2Cu_3O_{6.95}$ at 295, 100, and 12 K. In the normal state, the curves for $I(\omega)$ do not converge over the examined frequency range, which suggests that the midinfrared excita-

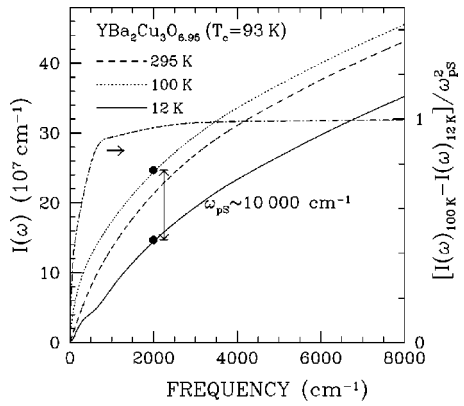

FIG. 2. I(ω) for $YBa_2Cu_3O_{6.95}$ at 295, 100, and 12 K from $\approx$50–8000 cm^{-1}, where $I(\omega)=(120/\pi)\int_0^{\omega}\sigma_1(\omega')d\omega'$ is the conductivity sum rule; $\omega_p^2=I(\omega\rightarrow\infty)$. The values for ω_p in the text have been obtained by integrating to a cutoff frequency of 8000 cm^{-1}, listed in Table I. The difference in the sum rules for $T\simeq T_c$ and $T\ll T_c$ is normalized with respect to ω_{pS}^2 in Table I (dot-dash line); this value quickly converges to unity above $\approx$800 cm^{-1}, indicating that the condensate in optimally doped materials is fully formed well below the cutoff frequency.

tions have a temperature dependence associated with them. We call this quantity infrared spectral weight, and the associated plasma frequency the infrared plasma frequency.

The integral has been truncated at $\omega_c=8000$ cm^{-1} ($\approx$1 eV). The resulting values for ω_p, which are listed in Table I, are quite sensitive to the choice of the cutoff frequency. The experimentally determined values for ω_p can be compared to the expected values. The measured carrier concentration in $YBa_2Cu_3O_{7-\delta}$ has been determined[37] to be $n_0\approx 6.2\times 10^{21}$ cm^{-3}. The plasma frequency $\omega_p=4\pi ne^2/m^*$, assuming that $m^*=m_e$, and that the carrier density along the chains is n_0, and perpendicular to the chains is $\frac{1}{2}n_0$ (if the holes are equally distributed between the chains and the planes), yields values of $\omega_{p,a}=16\,660$ cm^{-1} and $\omega_{p,b}=23\,570$ cm^{-1} in the optimally doped material. In a twinned sample, the observed plasma frequency will be a combination of the chains and the planes, $\omega_{p,ab}^2=(\omega_{p,a}^2+\omega_{p,b}^2)/2$, or $\omega_{p,ab}=20\,410$ cm^{-1}, which because of the choice of effective mass represents an *upper* limit for the plasma frequency. The values returned from the sum-rule estimates are actually slightly larger than these values. However, it is difficult to asses the relative contributions of the free-carrier to the mid-infrared components, so this result is not surprising. In any case, it should be noted that different values of ω_p simply scale the results for $1/\tau(\omega)$ and $m^*(\omega)/m$. The values of ω_p for the pure, lightly, and heavily doped materials are all within $\approx$700 cm^{-1} of each other ($\omega_p\approx 21\,000$ cm^{-1} at $T\gtrsim T_c$, using a cutoff frequency of 8000 cm^{-1}), indicating that the carrier concentration remains unaffected at these levels of nickel doping.

We also calculate a second spectral weight and plasma frequency, the Drude spectral weight ω_{pD}, by performing a nonlinear least-squares fit of the simple Drude conductivity with a constant scattering rate, to the optical conductivity at low frequency, just above T_c. While the Drude model does not describe the optical conductivity over a wide frequency range, by restricting the fit to low frequencies only (typically $\leqslant$500 cm^{-1}), an estimate of the spectral weight associated with the narrow free-carrier component may be determined.

The third spectral weight we calculate is that of the superconducting condensate ω_{pS} determined from the real part of the dielectric function for $T\ll T_c$ in the superconducting state. In a system where all of the normal-state carriers collapse into the superconducting delta function, the real part of the dielectric function in Eq. (1) becomes $\epsilon(\omega)=\epsilon_\infty'-\omega_{pS}^2/\omega^2$, where ω_{pS} is the plasma frequency of the condensate. The inset in Fig. 3 shows $\epsilon_1(\omega)$ vs ω^{-2} at 12 K for the three materials; linear regressions of the straight lines yield (with the penetration depths in brackets) $\omega_{pS}=9740\pm 400$ (1634 Å), 9140 ± 400 (1741 Å), and 7320 ± 300 cm^{-1} (2174 Å) for the nominally pure, light, and heavy Ni concentrations, respectively. The low value for ω_{pS} in the material with the heavy Ni concentrations indicates a sharp reduction in the strength of the condensate at 12 K. However, at 6 K the value for $\omega_{pS}=8730\pm 400$ cm^{-1} indi-

TABLE I. The estimated infrared (ω_p) and Drude plasma frequencies (ω_{pD}) for $T\simeq T_c$, and the plasma frequency of the superconducting condensate (ω_{pS}) for $T\ll T_c$, determined from an analysis of the real part of the dielectric function as well as optical-conductivity sum rules, for $YBa_2(Cu_{1-x}Ni_x)_3O_{6+y}$ twinned and detwinned single crystals, for $y=0.60$ and 0.95 oxygen dopings. (All units are in cm^{-1} unless otherwise noted.)

			$E\|ab$			$E\|a$			$E\|b$	
$YBa_2(Cu_{1-x}Ni_x)_3O_{6.95}$	T_c (K)	ω_p	(ω_{pD})	[ω_{pS}]	ω_p	(ω_{pD})	[ω_{pS}]	ω_p	(ω_{pD})	[ω_{pS}]
''pure''	93.2	21 360	(9660)	[9740]	16 990[a]	—	[9947][a]	26 600[a]	—	[14 470][a]
0.0075	91	20 590	(9580)	[9140]	16 710	(6610)	[8976]	23 380	(14 520)	[9130]
0.014	89	21 080	(10 580)	[7320][b]	—	—	—	—	—	—
			$E\|ab$			$E\|a$			$E\|b$	
$YBa_2(Cu_{1-x}Ni_x)_3O_{6.60}$	T_c (K)	ω_p	(ω_{pD})	[ω_{pS}]	ω_p	(ω_{pD})	[ω_{pS}]	ω_p	(ω_{pD})	[ω_{pS}]
''pure''	$\approx$59	—	—	—	14 090[c]	—	[6420][a]	21 390[c]	—	[8720][a]
0.0075	$\approx$57	—	—	—	13 250	(5510)	[5620]	19 710	(8330)	[5820]
0.014	$\approx$55	17 790	(6250)	[5280]	—	—	—	—	—	—

[a]These values were determined from the data in Ref. 32.

[b]The strength of the condensate is $\approx$8700 cm^{-1} at 6 K, indicating that the condensate still has some temperature dependence even for $T\ll T_c$.

[c]Measurements performed at McMaster (unpublished).

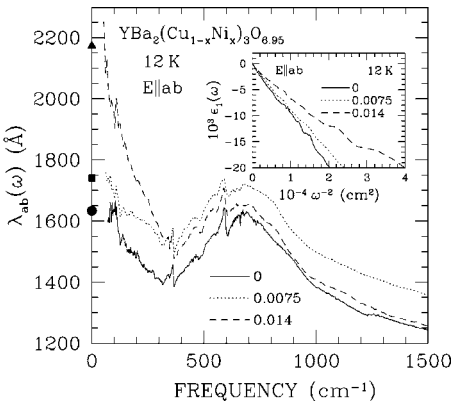

FIG. 3. The ab-plane frequency dependent penetration depth in $YBa_2(Cu_{1-x}Ni_x)_3O_{6.95}$, for the nominally pure material and several different Ni concentrations. At low frequency, $\lambda_{ab}(\omega)$ increases rapidly with increasing Ni concentration. The extrapolated values of $\lambda_{ab}(\omega\rightarrow 0)$ are in good agreement with the values determined from a plot of $\epsilon_1(\omega)$ vs ω^{-2} shown in inset; full circle, square, and triangle for 0, 0.0075, and 0.014 Ni concentrations, respectively.

cating that ω_{pS} still possesses some temperature dependence, even for $T \ll T_c$, in agreement with measurements of $\lambda(T)$ at microwave frequencies.[8] It is notable that the estimated Drude weight and the weight of the condensate are comparable, indicating that most of the spectral weight that collapses into the condensate originates at low frequencies. This effect is shown most clearly by the normalized spectral weight of the condensate shown in Fig. 2, which is calculated by taking the difference of the sum rules for $T \gtrsim T_c$ and $T \ll T_c$, and dividing by the value of condensate ω_{pS}^2 (Ref. 38); by ≈ 800 cm^{-1} this value has approached unity, indicating that nearly all of the *ab*-plane spectral weight has gone into the condensate.

The frequency dependent effective penetration depth $\lambda_{ab}^{-1}(\omega) = 2\pi\sqrt{\omega\sigma_2(\omega)}$ is shown in Fig. 3 from ≈ 50–1500 cm^{-1} for the nominally pure, light, and heavy Ni concentrations at 12 K. There is a rapid increase in $\lambda_{ab}(\omega)$ at low frequency with increasing Ni content. The extrapolated values of $\lambda_{ab}(\omega\rightarrow 0) \approx 1600$, 1800, and 2200 Å for the nominally pure, light, and heavy Ni concentrations, respectively, are in good agreement with the values for the penetration depth calculated above from the real part of the dielectric function (summarized in Table II).

The two most striking features in the optical conductivity that evolve with increasing Ni concentration are the low-frequency residual conductivity and the unusual shoulder seen in $\sigma_1(\omega)$ at ≈ 300 cm^{-1}. The increase in the low-frequency residual conductivity coincides with the decrease in the strength of the condensate below T_c, while the plasma frequency of the normal-state carriers stays essentially constant (see Table I).

B. Twin-free systems

1. Optimal oxygen doping: $YBa_2Cu_3O_{6.95}$

The optical conductivity for the detwinned single crystal of $YBa_2(Cu_{1-x}Ni_x)_3O_{6.95}$ for $x = 0.0075$ ($T_c = 91$ K) for $E \| a$ [$\sigma_{1a}(\omega)$] at 295, 100, and 12 K from ≈ 50–1500 cm^{-1} is shown in Fig. 4(a); the conductivity for $E \| b$ is shown for the same temperatures and over the same range in Fig. 4(b). The reflectance for $E \| a$ and $E \| b$ is shown in the insets from ≈ 50–1000 cm^{-1} in Figs. 4(a) and 4(b), respectively. Light polarized along the a axis probes just the CuO_2 planes, while light polarized along the b axis probes the CuO chains, as well as the CuO_2 planes.

TABLE II. The penetration depth $\lambda(T) = 1/2\pi\omega_{pS}(T)$(Å) at $T \ll T_c$ (≈ 12 K) in $YBa_2(Cu_{1-x}Ni_x)_3O_{6+y}$ twinned and detwinned single crystals, for $y = 0.60$ and 0.95 oxygen dopings.

Material		λ (Å)		
$YBa_2(Cu_{1-x}Ni_x)_3O_{6.95}$	T_c (K)	$E \| ab$	$E \| a$	$E \| b$
''pure''	93.2	1634	1600	1100
0.0075	91	1741	1773	1702
0.014	89	2174	—	—
$YBa_2(Cu_{1-x}Ni_x)_3O_{6.60}$	T_c (K)	$E \| ab$	$E \| a$	$E \| b$
''pure''	≈59	—	2480	1825
0.0075	≈57	—	2832	2735
0.014	≈55	3014	—	—

The overall nature of $\sigma_{1a}(\omega)$ in Fig. 4(a) is similar to that of $\sigma_1(\omega)$ in the same twinned sample in Fig. 1(b). However, in the normal state the Drude-like profile used to describe the carriers is much narrower than in the twinned sample. Below T_c the residual conductivity at low frequency is steadily decreasing with increasing frequency and reaches a minimum at ≈ 500 cm^{-1}. However, at low temperature the minimum in $\sigma_{1a}(\omega)$ is $\leqslant 500\ \Omega^{-1}$ cm^{-1}, which is less than half of

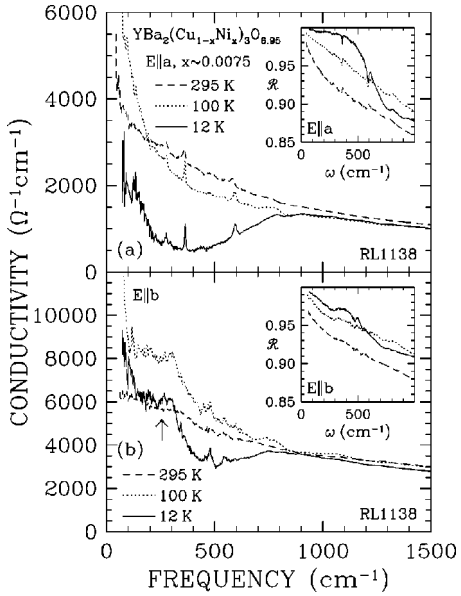

FIG. 4. (a) The optical conductivity for the detwinned single crystal $YBa_2(Cu_{1-x}Ni_x)_3O_{6.95}$ ($x = 0.0075$, $T_c = 91$ K) for radiation polarized along the a axis. This polarization probes just the CuO_2 planes. Note the lack of any feature at ≈ 300 cm^{-1}. (b) The optical conductivity for radiation polarized along the b axis. This polarization probes *both* the chains and the planes. Note the prominent feature at ≈ 300 cm^{-1} visible above and below T_c, and the large amount of residual conductivity at low frequency. Insets show the reflectance.

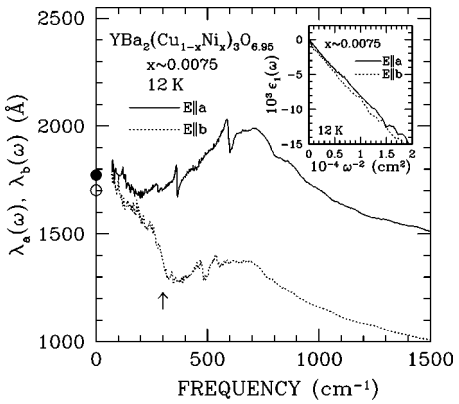

FIG. 5. The frequency dependent penetration depth in a detwinned single crystal of $YBa_2(Cu_{1-x}Ni_x)_3O_{6.95}$ for $x=0.0075$ ($T_c=91$ K). Note that $\lambda_a(\omega)>\lambda_b(\omega)$ over the illustrated frequency range, but below ≈ 300 cm^{-1} $\lambda_b(\omega)$ increases quickly (indicated by the arrow) and the values converge as $\omega\rightarrow 0$ to $\approx 1800\pm 100$ Å , for $E\|a$ and $E\|b$, shown as filled and open circles, respectively. Inset: A plot of $\epsilon_{1a}(\omega)$ and $\epsilon_{1b}(\omega)$ vs ω^{-2} at 12 K for $\omega\approx 50$–500 cm^{-1}. In the clean-limit case, the slope is ω_{pS}^2, which from a linear regression is $\omega_{pS}=8976\pm 400$ and 9130 ± 400 cm^{-1} for $E\|a$ and $E\|b$, respectively.

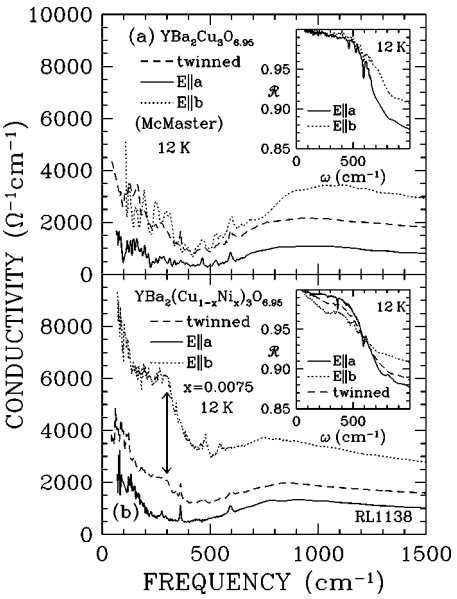

FIG. 6. (a) The optical conductivity for nominally pure twinned and detwinned single crystals of $YBa_2Cu_3O_{6.95}$. Note the absence of any feature in the optical conductivity in either the twinned or detwinned sample at ≈ 300 cm^{-1}. Inset: the reflectance at 12 K. (b) The optical conductivity for the twinned and detwinned crystal of $YBa_2(Cu_{1-x}Ni_x)_3O_{6.95}$ for $x=0.0075$. Note that the shoulder in $\sigma_1(\omega)$ seen at ≈ 300 cm^{-1} is only seen for $E\|b$ in the detwinned sample, and is absent for $E\|a$. Inset: the reflectance at 12 K.

that observed in $\sigma_1(\omega)$ in the twinned sample. The presence of Ni at the 0.0075 level seems to have very little effect on $\sigma_{1a}(\omega)$, and overall is very similar to $\sigma_{1a}(\omega)$ in studies of nominally pure, detwinned systems.[32,39] No spectral feature at ≈ 300 cm^{-1} is observed in this polarization.

The picture for $\sigma_{1b}(\omega)$ shown in Fig. 4(b) is dramatically different. The additional presence of chains along the *b*-axis direction results in an increase of the plasma frequency and a $\sigma_{1b}(\omega)$ that is considerably larger than $\sigma_{1a}(\omega)$, as expected. At room temperature, $\sigma_{1b}(\omega)$ is quite broad. However, for $T\gtrsim T_c$ some narrowing and transfer of spectral weight to low frequency has occurred, but what is unusual is that the shoulder at ≈ 300 cm^{-1}, which was previously observed only for $T\ll T_c$ in the twinned and detwinned samples,[39] is now clearly visible in the normal state; indications of this feature can also be seen in the reflectance. Below T_c, there is a decrease in the low-frequency conductivity associated with the formation of a superconducting condensate. The presence of the shoulder in $\sigma_{1b}(\omega)$ above and below T_c indicates that the ≈ 300 cm^{-1} shoulder is not feature of the superconducting state in Ni-doped $YBa_2Cu_3O_{6.95}$.

The frequency dependent penetration depth is shown in Fig. 5 for $YBa_2(Cu_{1-x}Ni_x)_3O_{6.95}$ with the light Ni concentration ($x=0.0075$,$T_c=91$ K) along the *a* and *b* axis at 12 K from ≈ 50–1500 cm^{-1}. For $\omega\gtrsim 300$ cm^{-1}, $\lambda_a(\omega)>\lambda_b(\omega)$. However at low frequency, $\lambda_b(\omega)$ increases rapidly to approach $\lambda_a(\omega)$, while $\lambda_a(\omega)$ remains relatively constant. The extrapolated values of $\lambda_a(\omega\rightarrow 0)\approx 1850\pm 100$ Å and $\lambda_b(\omega\rightarrow 0)\approx 1800\pm 100$ Å are in good agreement with the values the plasma frequency of the condensate (Table I) determined from $\epsilon_1(\omega)$, shown in Table II. The normal-state in-plane anisotropy as determined by the ratio of the plasma frequencies $\omega_{p,b}^2/\omega_{p,a}^2\approx 1.9$–$2.1$, is in good agreement with previous estimates.[32] However, the in-plane anisotropy below T_c taken from λ_a/λ_b, is ≈ 1.4 at high frequency, but as $\omega\rightarrow 0$ the materials become completely isotropic, suggesting that the superconductivity along the chains has been destroyed. The rapid increase in $\lambda_b(\omega)$ at low frequency is similar to that seen in $\lambda_{ab}(\omega)$ in the twinned samples, indicating that the behavior in the twinned systems is a reflection of the chain dynamics rather than the in-plane dynamics.

The inset in Fig. 5 shows the real part of the dielectric function for $E\|a$ and $E\|b$ vs ω^{-2} at 12 K; linear regressions yield values of $\omega_{pS}=8976\pm 400$ cm^{-1} (1773 Å) and $\omega_{pS}=9130\pm 400$ cm^{-1} (1702 Å) along the $E\|a$ and $E\|b$, polarizations, respectively. Thus within experimental error, there is no anisotropy in the *ab* plane as $\omega\rightarrow 0$.

At this point, it is useful to compare the results for the optical conductivity of a nominally pure, detwinned single crystal of $YBa_2Cu_3O_{6.95}$ grown by the same group with that of the twinned and detwinned material with a light Ni concentration. The optical conductivity of nominally pure $YBa_2Cu_3O_{6.95}$ at 12 K from ≈ 50–1500 cm^{-1} is shown in Fig. 6(a) for $E\|a$ and $E\|b$; while the results for $YBa_2(Cu_{1-x}Ni_x)_3O_{6.95}$ with a light Ni concentration ($x=0.0075$) at 12 K over the same frequency range for $E\|a$ and $E\|b$ are shown in Fig. 6(b). In both cases the results for the twinned crystal ($E\|ab$) have also been included. The insets show the reflectance at 12 K from ≈ 50–1000 cm^{-1} for both of the respective materials. These two materials have the same optimal oxygen doping, so the number of oxygen vacancies in the chains should be the same. However, in the nominally pure material, the $E\|a$ and $E\|b$ curves have a similar character, and there is no indication of a shoulder in any of the conductivity curves, including the twinned crystal for which the signal-to-noise ratio is quite good. In comparison, the shoulder in the conductivity is clearly visible in the twinned crystal with a light Ni concentration.

While the spectra for $E\|a$ in the nominally pure crystal and the crystal with a light Ni concentration look almost identical, the $E\|b$ curve for the Ni-doped material is *quite* different than its counterpart in the pure material; the shoulder at $\approx 300\ \mathrm{cm}^{-1}$ is quite prominent and the large amount of residual conductivity at low frequency has washed out the minima seen in $\sigma_{1b}(\omega)$ in the nominally pure crystal.

This comparison suggests a number of things. The absence of any feature at $\approx 300\ \mathrm{cm}^{-1}$ in the nominally pure detwinned $YBa_2Cu_3O_{6.95}$ system suggests that it is not due to oxygen vacancies, but rather to Ni impurities. The similarity of the conductivities in the copper-oxygen planes $[\sigma_{1a}(\omega)]$ for the nominally pure and lightly doped materials, when viewed in conjunction with the dramatically different conductivities along the chain direction $[\sigma_{1b}(\omega)]$ suggest that the CuO chains, which can apparently be viewed as one dimensional in character, are very sensitive to the presence of impurities, and that a significant fraction of the Ni appears to doping into chain sites.[25,26] However, it is difficult to estimate from these data the relative concentration of the Ni in chain and plane sites. The presence of Ni in the chain sites also leads to a sharp reduction in the strength of the superconducting condensate along the chain direction (Table I), and therefore the anisotropy of the Ni-doped material. This observation is consistent with the suggestion that it is the disorder (or impurities) in the chains[32] of $YBa_2Cu_3O_{7-\delta}$ that are responsible for the low anisotropies which have been observed in early studies of these materials.[40]

From an examination of the twinned sample with the heavy Ni concentration, it is clear that the position of the $\approx 300\ \mathrm{cm}^{-1}$ feature does not shift with increasing Ni doping. However, it is important to examine both nominally pure and Ni-doped, detwinned oxygen-reduced samples to determine if the position of this feature is sensitive to oxygen content.

2. Oxygen underdoped: $YBa_2Cu_3O_{6.60}$

The detwinned sample (RL1138) has been oxygen-reduced to $YBa_2(Cu_{1-x}Ni_x)_3O_{6.60}$ for the light Ni concentration ($x=0.0075$), with an estimated $T_c \approx 57$ K. Note that T_c has only been measured directly for the pure oxygen-reduced material, $T_c = 59$ K. In view of the effect of Ni incorporation on T_c in the optimally doped materials, it is likely that that the T_c of the lightly doped, oxygen-reduced material is suppressed by ≈ 2 K. However, this has not been explicitly measured. The optical conductivity for $E\|a$ at 295, 70, and 12 K from ≈ 50–$1500\ \mathrm{cm}^{-1}$ is shown in Fig. 7(a); the reflectance for the same temperatures from ≈ 50–$1000\ \mathrm{cm}^{-1}$ is shown in the inset. The overall value of $\sigma_{1a}(\omega)$ is much lower than is observed in the material with optimal-oxygen doping due to the decrease in the number of carriers in the planes; the extrapolated value of $\sigma_{1a}(\omega \to 0) \approx 1600\ \Omega^{-1}\ \mathrm{cm}^{-1}$, while it is $\gtrsim 4500\ \Omega^{-1}\ \mathrm{cm}^{-1}$ in the optimally doped material with the same Ni content. The minimum in the conductivity for $T \ll T_c$ has not changed position, and is still $\approx 500\ \Omega^{-1}\,\mathrm{cm}^{-1}$, which appears to be a general feature of these materials.[41,42] There are a number of features in $\sigma_{1a}(\omega)$ that are associated with phonons, but an unusual weak feature at $\approx 300\ \mathrm{cm}^{-1}$ may now also be distinguished at low temperature. However, this feature is *not* seen in the normal state, so it is uncertain if it is related to the feature seen at the same frequency in the chains.

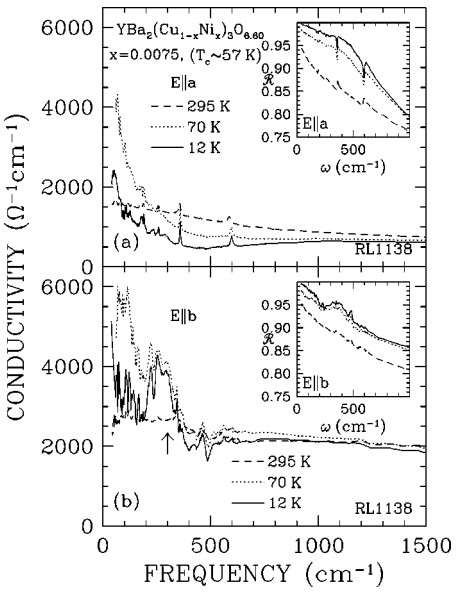

FIG. 7. (a) The *a*-axis conductivity for oxygen-reduced $YBa_2(Cu_{1-x}Ni_x)_3O_{6.60}$ for $x=0.0075$ ($T_c \approx 57$ K). Inset: the reflectance at 295, 70, and 12 K. (b) The *b*-axis conductivity. The feature at $\approx 300\ \mathrm{cm}^{-1}$ is now quite prominent above and below T_c. Inset: the reflectance at 295, 70, and 12 K.

The optical properties along the *b* axis of the underdoped material are quite different from those of the CuO_2 planes. The conductivity for $E\|b$ at 295, 70, and 12 K from ≈ 50–$1500\ \mathrm{cm}^{-1}$ is shown in Fig. 7(b); the reflectance for the same temperatures from ≈ 50–$1000\ \mathrm{cm}^{-1}$ is shown in the inset. At room temperature, $\sigma_{1b}(\omega)$ is quite flat. Just above T_c the low-frequency component of the conductivity has narrowed, but it appears that the response observed is commensurate with the narrowing that is observed in CuO_2 planes $[\sigma_{1a}(\omega)]$, which cannot be distinguished from the chains in this polarization. Below T_c, there is a slight collapse of the conductivity at low frequency due to a transfer of spectral weight into the condensate, but it also appears that this response is due entirely to the planes. In the normal state there is a feature at $\approx 300\ \mathrm{cm}^{-1}$ which becomes quite prominent at $T \gtrsim T_c$, but does not appear to change in position or strength below T_c.

A comparison between the frequency dependent penetration depths along the *a* and *b* axis is shown in Fig. 8 at 12 K from ≈ 50–$1500\ \mathrm{cm}^{-1}$. As in the case of the optimally doped materials $\lambda_a(\omega)$ is essentially frequency independent and $\lambda_b(\omega)$ is equal to $\lambda_a(\omega)$ at zero frequency, but $\lambda_b(\omega)$ decreases rapidly with increasing frequency. The zero-frequency penetration depths agree with those calculated from the plasma frequency of the condensate (shown in Tables I and II). The inset in Fig. 8 shows $\epsilon_{1a}(\omega)$ and $\epsilon_{1b}(\omega)$ vs ω^{-2} at 12 K; a linear regression of the straight line yields $\omega_{pS} = 5620 \pm 300\ \mathrm{cm}^{-1}$ and $5820 \pm 300\ \mathrm{cm}^{-1}$ for $E\|a$ and $E\|b$, respectively.

C. Chain conductivity

It has been proposed that the conductivity along the chains may be determined by $\sigma_{ch}(\omega) = \sigma_{1b}(\omega) - \sigma_{1a}(\omega)$

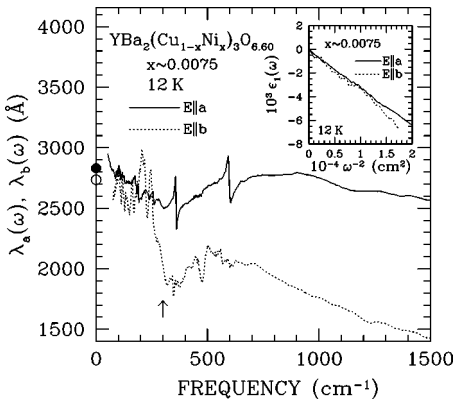

FIG. 8. The frequency dependent penetration depth in a detwinned single crystal of oxygen-reduced $YBa_2(Cu_{1-x}Ni_x)_3O_{6.60}$ for $x=0.0075$ ($T_c \approx 57$ K). Note that $\lambda_a(\omega) > \lambda_b(\omega)$ over the illustrated frequency range, but below ≈ 300 cm^{-1} $\lambda_b(\omega)$ increases quickly (indicated by the arrow) and the values converge as $\omega \to 0$ to $\approx 2800 \pm 200$ Å, for $E \| a$ and $E \| b$, shown as filled and open circles, respectively. Inset: a plot of $\epsilon_{1a}(\omega)$ and $\epsilon_{1b}(\omega)$ vs ω^{-2}; linear regressions yield $\omega_{pS}=5620 \pm 300$ cm^{-1} and $\omega_{pS}=5820 \pm 300$ cm^{-1}, for $E \| a$ and $E \| b$, respectively.

(Ref. 22). The chain conductivity determined in this manner is shown in Fig. 9(a) for $YBa_2(Cu_{1-x}Ni_x)_3O_{6.95}$ for $x=0.0075$ at 295, 100, and 12 K and in Fig. 9(b) for $YBa_2(Cu_{1-x}Ni_x)_3O_{6.60}$ for the same light Ni concentration at 295, 70, and 12 K from ≈ 50–1000 cm^{-1}. As Fig. 9(a) shows, apart from a scale factor the chain conductivity is very similar for the two doping levels: the room-temperature conductivity is flat but a peak develops at low temperature with a sharp drop at ≈ 300 cm^{-1}. The overall scale factor

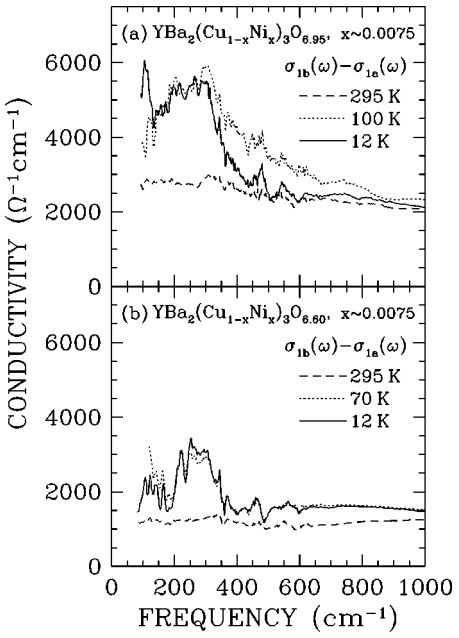

FIG. 9. (a) The optical conductivity along the chains $[\sigma_{1b}(\omega) - \sigma_{1a}(\omega)]$ for the detwinned optimally doped $YBa_2(Cu_{1-x}Ni_x)_3O_{6.95}$ material with the light Ni concentration. (b) The optical conductivity along the chains for the oxygen-reduced material with the same Ni concentration at 295, 70, and 12 K from ≈ 50–1000 cm^{-1}. Note the absence of any temperature dependence through T_c.

that would make the two sets of spectra collapse on top of one another is ≈ 1.6, which, within experimental error, is precisely the ratio of the number of chain oxygens for the two compositions 6.95 and 6.60, namely 1.58. The same behavior is also observed in the pure materials for the same two oxygen stiochiometries, where the conductivity ratio in the midinfrared along the chain direction is again ≈ 1.6. Thus we are led to the conclusion that the properties of the chains are independent of doping in this range of oxygen concentrations; the only effect of oxygen is to add to the number and length of the chain fragments. This view is in agreement with the results of x-ray absorption fine structure, where it is found that above a composition of 6.50, the average valence of the chain oxygens does not change.[43]

The temperature dependence of $\sigma_{1b}(\omega)$ in Fig. 4(b) appears to originate only partly from the chains. As Fig. 9(a) shows, the conductivity along the chains at 295 K is essentially frequency independent. The only change in the conductivity that occurs with decreasing temperature is related almost entirely to the feature at ≈ 300 cm^{-1}; this feature is entirely absent at 295 K, and reaches full strength above T_c. With the exception of some residual conductivity at low frequency, there appears to be little change in $\sigma_{ch}(\omega)$ below T_c. If the localized carriers exhibited a broad mid-infrared absorption, then optical-conductivity sum-rule calculations in the normal state would not be able to distinguish between a free-carrier component and localized carriers. As Table I indicates, for the cutoff frequencies examined, there is no appreciable decrease in the value returned by the sum rule at the cutoff frequency upon Ni incorporation. However, if the carriers are localized on the Ni sites in the chains, then this provides an alternative to strong pair breaking to explain the decrease in the strength of the condensate along the chains below T_c (Table I).

In Fig. 9(b), the oxygen-underdoped sample with the same Ni doping, the room-temperature conductivity is frequency independent. Except for a slight uniform increase in the conductivity, the most dramatic change with decreasing temperature is the appearance of the feature at ≈ 300 cm^{-1}; entirely absent at 295 K, it is fully formed at $T \gtrsim T_c$ (this behavior is identical to the material with optimal oxygen doping). Below T_c, there is essentially no change in $\sigma_{1b}(\omega)$ over the entire low-frequency range. As in the previous case, this suggests that the conductivity at low frequency along the chains is not metallic and that the presence of Ni has totally destroyed the superconductivity along the chains. This effect can also be inferred from the plasma frequency of the condensate; if $\omega_{pS,ch}^2 = \omega_{pS,b}^2 - \omega_{pS,a}^2$ then in the nominally pure material with optimal oxygen doping $\omega_{pS,ch} \approx 10\,500$ cm^{-1}, but in the optimally doped material with a light Ni concentration $\omega_{pS,ch} \approx 1670$ cm^{-1}, which is only 3% of the condensate density of the pure material. A similar behavior is observed in the underdoped material, where the nominally pure material yields $\omega_{pS,ch} \approx 5900$ cm^{-1}, while the same material with the light Ni concentration has $\omega_{pS,ch} \approx 1510$ cm^{-1}, only 7% of the condensate density of the nominally pure, undoped material. The fact that the inferred conductivity along the chains for the optimally doped and underdoped materials with the light Ni concentration [Figs. 9(a) and 9(b)] is almost frequency independent, suggests either carrier localization or very strong elastic scattering has

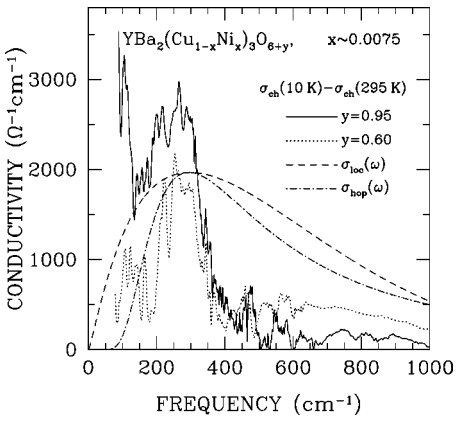

FIG. 10. The conductivity along the chain direction with the room-temperature contribution removed, $\sigma_{ch}(10\ \mathrm{K}) - \sigma_{ch}(295\ \mathrm{K})$ [where $\sigma_{ch}(\omega) = \sigma_{1b}(\omega) - \sigma_{1a}(\omega)$], from ≈ 60–$1000\ \mathrm{cm}^{-1}$ for $YBa_2(Cu_{1-x}Ni_x)_3O_{6+x}$ for $x = 0.0075$, $y = 0.95$ (optimally doped), and $y = 0.60$ (underdoped). The two calculated curves depict the conductivity due to a localization process [σ_{loc}, from Eq. (4)], and a hopping process [σ_{hop}, from Eq. (5)]. Both curves have been scaled to illustrate their functional forms, and are intended only as a guide to the eye.

destroyed the coherent Drude peak. In accord with this, there is a nearly complete absence of superconductivity in the chains. It is striking that while the relatively low Ni concentration has little effect on the superconductivity on the planes, it is enough to destroy the condensate on the chains.

To display the feature at $300\ \mathrm{cm}^{-1}$ more clearly, in Fig. 10 we subtract out the room-temperature incoherent background, and plot $\sigma_{ch}(10\ \mathrm{K}) - \sigma_{ch}(295\ \mathrm{K})$ for the material with the light Ni concentration, for the optimally and oxygen underdoped systems.

IV. DISCUSSION

A. Localization and hopping

In what follows we focus on the chains since, at the low level of doping of our samples, the conductivity of the CuO_2 planes is unaffected by the nickel impurities, and all the *a*-axis spectra look the same in the detwinned samples, with the optical properties being determined by solely by oxygen content. The incorporation of Ni into these materials was initially thought to occur mainly in the CuO_2 planes. However, the profound effect of the Ni upon the conductivity along the chains indicates that a substantial amount of Ni is in fact doping into the chains. While highly ordered chains are expected to exhibit metallic properties,[32,44] the failure of the chains to display a Drude-like response shows that the presence of even a small concentration of Ni impurities in the chains has destroyed not only the coherent metallic behavior of the chains but also their superconductivity. In what follows we discuss several models that yield such incoherent response. We start by summarizing what is known about the $300\ \mathrm{cm}^{-1}$ feature, the most striking manifestation of Ni doping in the *b*-axis conductivity spectra.

The feature at $300\ \mathrm{cm}^{-1}$ has been observed in the thin-film absorptivity,[45] but is not reproducible. A recent study of radiation damage in single crystals[23] also shows a shoulder at $\sigma_1(\omega)$ at $\approx 300\ \mathrm{cm}^{-1}$, but this feature was not consistently observed. In the twinned samples examined here, there is no indication of this shoulder in the normal state, which initially led to the suggestion that this may be a feature of the superconducting state. Also, recent calculations of the optical conductivity of a dirty *d*-wave superconductor predict such a shoulder in the conductivity in the region of twice the maximum value for the gap.[10]

While studies of nominally pure, twinned, and detwinned $YBa_2Cu_3O_{7-\delta}$ crystals generally do not indicate any structure in the $300\ \mathrm{cm}^{-1}$ region,[32] there has been a report of a feature in this approximate region for $T \ll T_c$ along the chain direction in a *detwinned* crystal. In this study by Schützmann *et al.* on a detwinned $YBa_2Cu_3O_{7-\delta}$ crystal,[39] it was suggested that oxygen vacancies at low temperatures were strong backscattering barriers for the carriers in the chains, and that the feature at $300\ \mathrm{cm}^{-1}$ was due to thermally activated hopping across oxygen defects in the chains.[39] On the other hand, there have been a number of studies on substitutions for Cu by Fe, Co, Al, and Au in $YBa_2Cu_3O_{7-\delta}$ (Refs. 46–48), which suggest that these impurities dope primarily into the chains, creating disorder and forming fragments. There is also evidence that in $PrBa_2Cu_3O_{7-\delta}$, where the hole doping in the chains is expected to be the same as in the Y-based material, there is strong carrier localization in the chains,[49] leading to a large peak in the optical conductivity at $\approx 1600\ \mathrm{cm}^{-1}$ at low temperatures.[50]

A system of carriers in the presence of a large amount of disorder can give rise to a conductivity peak through resonant phononless absorption.[51] The optical conductivity for this process at low temperature is[52,53]

$$\sigma_{loc}(\omega) = \frac{\pi^2}{3} e^2 g_0^2 \hbar \omega^2 a r_\omega^4, \qquad k_B T \ll \hbar\omega, \tag{4}$$

where a is the localization length, g_0 is the density of states, and $r_\omega = a \ln(\Omega_0/\omega)$, where Ω_0 is a measure of the overlap between the two localized states, and will be model dependent. The frequency dependence of this expression is $\sigma_{loc}(\omega) \propto \omega^2 [\ln(\Omega_0/\omega)]^4$, which gives a broad absorption peak with a maximum at $\Omega_0/\exp(2)$. This form of the conductivity is shown in Fig. 10 (dashed line) for $\Omega_0 \approx 2200\ \mathrm{cm}^{-1}$, which gives a peak centered at $\approx 300\ \mathrm{cm}^{-1}$. The conductivity increases rapidly, but falls off rather slowly at high frequency, in contrast to the rapid decrease of the high-frequency conductivity in the optimally doped material, as well as the oxygen-underdoped materials. Furthermore, other evidence for localization in the chains includes the so called ''chain peak,''[19,22,40,50] which is seen at much higher frequencies ($\approx 2000\ \mathrm{cm}^{-1}$) than the peak at $\approx 300\ \mathrm{cm}^{-1}$ observed in both the optimally doped, as well as the oxygen-underdoped material, in this work.

While detailed calculations have been performed for the optical conductivity have been performed on disordered chains,[54] an analytic expression for the hopping conductivity along a chain (at low temperature) is given by[55]

$$\sigma_{hop}(\omega) = 4\pi^2 c \epsilon_0 \omega_{p,b}^2 \omega_0^2 \omega^{-3} \sinh^{-1}\left(\frac{\pi\omega_0}{\omega}\right), \tag{5}$$

where ω_0 is the frequency of the hopping excitation, and $\omega_{p,b}$ is the plasma frequency of the carriers in the chains. This form of $\sigma_{hop}(\omega)$ will have a maximum at ω_0

$\approx v_F/(cl_b)$, where v_F is the Fermi velocity, and l_b is the mean-free path of the carriers in the chains.

The hopping conductivity, which is calculated and shown in Fig. 10 for $\omega_{p,ch}=5500\ \mathrm{cm}^{-1}$ and $\omega_0=280\ \mathrm{cm}^{-1}$ (dot-dash line), provides a somewhat better description of the conductivity along the chains. Thus it may be the case that the Ni impurities act as barriers for forward scattering in the way that oxygen vacancies were originally thought to.

The hopping conductivity has been calculated in Fig. 10 only for low temperature, or $k_BT \ll \hbar\omega_0$, where $\omega_0 \approx 300\ \mathrm{cm}^{-1}$ is the frequency of the hopping excitation. At room temperature ($\approx 210\ \mathrm{cm}^{-1}$) where $k_BT \approx \hbar\omega_0$ there will be a large amount of thermally excited hopping and the frequency dependence of the hopping conductivity will be strongly reduced; at 100 K ($\approx 70\ \mathrm{cm}^{-1}$) $k_BT < \hbar\omega_0$ and the response should then be expected to follow the form of Eq. (5). This yields the expected temperature dependence of this feature.

B. Chain-to-bilayer and interbilayer scattering?

There is another possible, more speculative origin of the feature at $\approx 300\ \mathrm{cm}^{-1}$. The assumption that scattering can occur *only* along the chains is restrictive, and it is possible that the carriers in the chains are also being scattered at the Ni impurity sites into the CuO_2 bilayers (and perhaps other chains), thereby coupling to the *c*-axis transport. As originally pointed out by Anderson[56] this mechanism transforms an enhanced *conductivity* in the *ab* plane to an enhanced *resistivity* in the *c*-axis direction. In the light of this it is significant that the location of the *peak* in $\sigma_{ch}(\omega)$ at $\approx 300\ \mathrm{cm}^{-1}$ is almost identical to the value of the *pseudogap* in the conductivity along the *c* axis, which has been observed in $YBa_2Cu_3O_{6+y}$ for $y \leq 0.9$ (''underdoped'') materials,[57] at ≈ 280–$310\ \mathrm{cm}^{-1}$. Two important characteristics of the *c*-axis pseudogap are (i) that it develops in the normal state primarily between room temperature and T_c, and (ii) that its position is not sensitive to the level of oxygen doping. The shoulder in $\sigma_{1b}(\omega)$ [or $\sigma_{ch}(\omega)$] is also observed to develop in the normal state and the position of the shoulder does not change with oxygen doping.

The shoulder is observed in the chains at the same position in the optimally doped material as the feature observed in the underdoped system. However, this presents a difficulty as no pseudogap is expected in the optimally doped system. This would imply that the Ni doping into the chains creates the local conditions necessary for a *c*-axis pseudogap, thus the preferential scattering at Ni sites will produce the same general feature, regardless of the oxygen content. There is reason to believe that this may indeed be the case. Measurements of Zhao *et al.* (see Fig. 10 in Ref. 58) suggest that Ni doping has the effect of reducing the carrier concentration,[58] an effect that at first glance is unexpected since in its normal valence state, Ni is expected to be a hole dopant. Nevertheless, the magnitude of the effect is such as to reduce the doping level in the limit of $x=1$ (the total substitution of Ni for Cu), from 6.95 to 6.60. The assertion that the substitution of Ni into a Cu(1) site creates the local conditions for a pseudogap is, however, speculative and thus this argument must be viewed as weaker than the localization and thermally activated hopping arguments.

V. CONCLUSIONS

The optical properties of twinned and detwinned single crystals of nominally pure and Ni-doped $YBa_2Cu_3O_{6+y}$, for ($y=0.95$) and oxygen underdoped ($y=0.60$) materials, have been examined over a wide frequency range, above and below T_c.

In the detwinned systems, Ni destroys the low-frequency conductivity in the chains [suggesting that there is a substantial amount of Ni being incorporated into the Cu(1) chain sites]. The sharp reduction of the condensate along the chain direction strongly reduces the *ab*-plane anisotropy below T_c, and indicates that the chains are not superconducting. The incorporation of Ni does not appear to have an effect on the conductivity in the CuO_2 planes.

A feature at $\approx 300\ \mathrm{cm}^{-1}$ is observed *only* along the chain direction, and is present above and below T_c indicating that it is not associated with the superconducting transition. If the Ni sites are strong backscattering barriers, then the shape and temperature dependence of the conductivity are described fairly well by a thermally activated hopping model. Alternatively, the proximity of this feature to the pseudogap along the *c* axis suggests that there may be strong scattering due to the Ni impurities out of the chains into the bilayers which allows the chains to couple to the *c*-axis electrodynamics; this explanation requires that Ni create the local conditions for a pseudogap along the *c* axis.

ACKNOWLEDGMENTS

The authors would like to acknowledge many useful discussions with V. J. Emery, A. V. Puchkov, and M. Strongin. We are grateful to A. W. McConnell, J. Rechner, and Q. Song for assistance in the laboratory. D.N.B. was supported by the Research Corporation. This work was supported by the Natural Sciences and Engineering Research Council of Canada, the Canadian Institute for Advanced Research, the Linville Institute, Simon Fraser University, the Department of Energy, Division of Materials Research under Contract No. DE-AC02-98CH10886, and NSF DMR 9875980.

*Electronic address: homes@bnl.gov

[1] For example, see *Physical Properties of High-Temperature Superconductors*, edited by D.M. Ginsberg (World Scientific, Singapore, 1989-1995),Vols.1–5, and references contained therein.

[2] D.B. Tanner and T. Timusk, in *Physical Properties of High-Temperature Superconductors III*, edited by D.M. Ginsberg (World Scientific, Singapore, 1992).

[3] J. Orenstein, G.A. Thomas, A.J. Millis, S.L. Cooper, D.H. Rapkine, T. Timusk, L.F. Schneemeyer, and J.V. Waszczak, Phys. Rev. B **42**, 6342 (1990); Z. Schlesinger, R.T. Collins, F. Holtzberg, C. Feild, G. Koren, and A. Gupta, *ibid.* **41**, 11 237 (1990).

[4] S.L. Cooper, D. Reznik, A. Kotz, M.A. Karlow, R. Liu, M.V. Klein, W.C. Lee, J. Giapintkis, D.M. Ginsberg, B.W. Veal, and A.P. Paulikas, Phys. Rev. B **47**, 8233 (1993).

[5] R. Liang, P. Dosanjh, D.A. Bonn, D.J. Baar, J.F. Carolan, and

W.N. Hardy, Physica C **195**, 51 (1992).
[6] W.N. Hardy, D.A. Bonn D.C. Morgan, R. Liang, and K. Zhang, Phys. Rev. Lett. **70**, 3999 (1993).
[7] Z.-X. Shen, D.S. Dessau, B.O. Wells, D.M. King, W.E. Spicer, A.J. Arko, D. Marshall, L.W. Lombardo, A. Kapitulnik, P. Dickinson, S. Doniach, J. DiCarlo, A.G. Loeser, and C.H. Park, Phys. Rev. Lett. **70**, 1553 (1993).
[8] D.A. Bonn, S. Kamal, K. Zhang, R. Liang, D.J. Baar, E. Klein, and W.N. Hardy, Phys. Rev. B **50**, 4051 (1994).
[9] L.S. Borkowski and P.J. Hirschfeld, Phys. Rev. B **49**, 15 404 (1994).
[10] J.P. Carbotte, C. Jiang, D.N. Basov, and T. Timusk, Phys. Rev. B **51**, 11 798 (1995).
[11] E.R. Ulm, J.-T. Kim, T.R. Lemberger, S.R. Foltyn, and X. Wu, Phys. Rev. B **51**, 9193 (1995).
[12] M.J. Sumner, J.-T. Kim, and T.R. Lemberger, Phys. Rev. B **47**, 12 248 (1993).
[13] J.-T. Kim, T.R. Lemberger, S.R. Foltyn, and X. Wu, Phys. Rev. B **49**, 15 970 (1994).
[14] J.-T. Kim, J. Giapintzakis, and D.M. Ginsberg, Phys. Rev. B **53**, 5922 (1996).
[15] K. Mizuhashi, K. Takenaka, Y. Fukuzumi, and S. Uchida, Phys. Rev. B **52**, R3884 (1995).
[16] B. Jayaram, S.K. Agarwal, C.V. Narasimha Rao, and A.V. Narlikar, Phys. Rev. B **38**, R2903 (1988).
[17] A.V. Mahajan, H. Alloul, G. Collin, and J.F. Marcone, Phys. Rev. Lett. **72**, 3100 (1994).
[18] D.A. Bonn, S. Kamal, A. Bonakdarpour, R. Liang, W.N. Hardy, C.C. Homes, D.N. Basov, and T. Timusk, Czech. J. Phys. **46**, 3195 (1996).
[19] H. Shibata, K. Semba, A. Matsuda, and T. Yamada, Phys. Rev. B **51**, 9294 (1995).
[20] N.L. Wang, S. Tajima, A.I. Rykov, and K. Tomimoto, Phys. Rev. B **57**, R11 081 (1998).
[21] D.N. Basov, B. Dabrowski, and T. Timusk, Phys. Rev. Lett. **81**, 2132 (1998).
[22] L.D. Rotter, Z. Schlesinger, R.T. Collins, F. Holtzberg, C. Field, U.W. Welp, G.W. Crabtree, J.Z. Liu, Y. Fang, K.G. Vandervoort, and S. Fleshler, Phys. Rev. Lett. **67**, 2741 (1991).
[23] D.N. Basov, A.V. Puchkov, R.A. Hughes, T. Strach, J. Preston, T. Timusk, D.A. Bonn, R. Liang, and W.N. Hardy, Phys. Rev. B **49**, 12 165 (1994).
[24] S.A. Hoffman, M.A. Castro, G.C. Follis, and S.M. Durbin, Phys. Rev. B **49**, 12 170 (1994).
[25] R.S. Howland, T.H. Geballe, S.S. Laderman, A. Fischer-Colbrie, M. Scott, J.M. Tarascon, and P. Barboux, Phys. Rev. B **39**, 9017 (1989).
[26] B.D. Padalia, S.J. Gurman, P.K. Mehta, and O. Prakash, Physica C **4**, 6856 (1992).
[27] C.C. Homes, Q. Song, B.P. Clayman, D.A. Bonn, R. Liang, W.N. Hardy, Proc. SPIE **2696**, 101 (1996).
[28] P. Schleger, W.N. Hardy, and B.X. Yang, Physica C **176**, 261 (1991).
[29] C.C. Homes. M. Reedyk, D.A. Crandles, and T. Timusk, Appl. Opt. **32**, 2976 (1993).
[30] D. Miller and P.L. Richards, Phys. Rev. B **47**, 12 308 (1993).
[31] H. Romberg, N. Nücker, J. Fink, Th. Wolf, X.X. Xi, B. Koch, H.P. Geserich, M. Dürrler, W. Assmus, and B. Gegenheimer, Z. Phys. B **78**, 367 (1990).
[32] D.N. Basov, R. Liang, D.A. Bonn, W.N. Hardy, B. Dabrowski, M. Quijada, D.B. Tanner, J.P. Rice, D.M. Ginsberg, and T. Timusk, Phys. Rev. Lett. **74**, 598 (1995).
[33] D.N. Basov, R. Liang, B. Dabrowski, D.A. Bonn, W.N. Hardy, and T. Timusk, Phys. Rev. Lett. **77**, 4090 (1996).
[34] A. Puchkov, D.N. Basov, and T. Timusk, J. Phys.: Condens. Matter **8**, 10 049 (1996).
[35] D.Y. Smith, in *Handbook of Optical Constants of Solids*, edited by E.D. Palik (Academic Press, New York, 1985), pp. 35–68.
[36] J. Kircher, M.K. Kelley, S. Rashkeev, M. Alouani, D. Fuchs, and M. Cardona, Phys. Rev. B **44**, 217 (1991).
[37] T.R. Chien, D.A. Brawner, Z.Z. Wang, and N.P. Ong, Phys. Rev. B **43**, 6242 (1991).
[38] D.N. Basov, S.I. Woods, A.S. Katz, E.J. Singley, R.C. Dynes, M. Xu, D.G. Hinks, C.C. Homes, and M. Strongin, Science **283**, 49 (1999).
[39] J. Schützmann, B. Gorshunov, K.F. Renk, J. Münzel, A. Zibold, H.P. Geserich, A. Erb, and G. Müller-Vogt, Phys. Rev. B **46**, 512 (1992).
[40] Z. Schlesinger, R.T. Collins, F. Holtzberg, C. Feild, S.H. Blanton, U. Welp, G.W. Crabtree, Y. Fang, and J.Z. Liu, Phys. Rev. Lett. **65**, 801 (1990).
[41] G.A. Thomas, J. Orenstein, D.H. Rapkine, M. Capizzi, A.J. Millis, R.N. Bhatt, L.F. Schneemeyer, and J.V. Waszczak, Phys. Rev. Lett. **61**, 1313 (1988).
[42] T. Timusk, D.N. Basov, C.C. Homes, A.V. Puchkov, and M. Reedyk, J. Supercond. **8**, 437 (1995).
[43] A. Bianconi (private communication).
[44] R. Fehrenbacher and T.M. Rice, Phys. Rev. Lett. **70**, 3471 (1993).
[45] D. Miller, P.L. Richards, S. Etemad, A. Inam, T. Venkatesan, B. Dutta, X.D. Wu, C.B. Eom, T.H. Geballe, N. Newman, and B.F. Cole, Phys. Rev. B **47**, 8076 (1994).
[46] A.R. Moodenbaugh, C.Y. Yang, Yimei Zhu, R.L. Sabatini, D.A. Fischer, Youwen Xu, and M. Suenaga, Phys. Rev. B **44**, 6991 (1991).
[47] Marta Z. Cieplak, Gang Ziao, C.L. Chien, A. Bakhshai, D. Artymowicz, W. Bryden, J.K. Stalick, and J.J. Rhyne, Phys. Rev. B **42**, 6200 (1990).
[48] A. Zibold, M. Dürrler, H.P. Geserich, A. Erb, and G. Müller-Vogt, Physica C **171**, 151 (1990).
[49] B. Grevin, Y. Berthier, G. Collin, and P. Mendels, Phys. Rev. Lett. **80**, 2405 (1998).
[50] K. Takenaka, Y. Imanaka, K. Tamasaku, T. Ito, and S. Uchida, Phys. Rev. B **46**, 5833 (1992).
[51] S. Tanaka and H.Y. Fan, Phys. Rev. **142**, 1516 (1963).
[52] B.I. Shklovskii and A.L. Efros, Zh. Éksp. Teor. Fiz. **81**, 406 (1981) [Sov. Phys. JETP **54**, 218 (1981)].
[53] A.L. Efros and B.I. Shklovskii, in *Electron-Electron Interactions in Disordered Systems*, edited by A.L. Efros and M. Pollak (North-Holland, Amsterdam, 1985).
[54] R. Fehrenbacher, Phys. Rev. B **49**, 12 230 (1994).
[55] A.A. Gogolin, Phys. Rep. **86**, 1 (1982).
[56] P.W. Anderson and Z. Zou, Phys. Rev. Lett. **60**, 132 (1988); P.W. Anderson, Phys. Rev. B **42**, 2624 (1990).
[57] C.C. Homes, T. Timusk, R. Liang, D.A. Bonn, and W.N. Hardy, Phys. Rev. Lett. **71**, 1645 (1993); C.C. Homes, T. Timusk, D.A. Bonn, R. Liang, and W.N. Hardy, Physica C **254**, 265 (1995).
[58] Y. Zhao, H.K. Liu, G. Yang, and S.X. Dou, J. Phys.: Condens. Matter **5**, 3623 (1993).